PERGAMON

Electrochimica Acta 47 (2001) 501–508

ELECTROCHIMICA Acta

www.elsevier.com/locate/electacta

On the origin of oscillations in the electrocatalytic oxidation of HCOOH on a Pt electrode modified by Bi deposition

Jaeyoung Lee *, Peter Strasser, Markus Eiswirth, Gerhard Ertl

Department of Physical Chemistry, Fritz-Haber-Institut der Max-Planck-Gesellschaft, Faradayweg 4-6, D-14195 Berlin, Germany

Received 21 May 2001; received in revised form 10 July 2001

Abstract

We report experimental observations on the temporal dynamics in the electrocatalytic oxidation of formic acid (HCOOH) on a polycrystalline Pt electrode modified by deposition of bismuth. Bismuth modification significantly enhanced the current density of HCOOH oxidation, since it suppressed the poisoning branch and increased the apparent direct oxidation rate. Impedance spectroscopy and the galvanostatic scan in HCOOH oxidation on Bi/Pt exhibited a hidden negative differential resistance and a Hopf bifurcation. The electrocatalytic oxidation of HCOOH on Bi/Pt spontaneously underwent transitions from homogeneous catalytic activity to spatiotemporally inhomogeneous distributions of the interfacial electrode potential, in the form of traveling pulses of the interfacial potential.

Keywords: Electrocatalytic oxidation; Formic acid; Bi/Pt electrode; Galvanostatic oscillations; Hidden negative impedance

1. Introduction

The electro-oxidation of small organic molecules such as formic acid (FA), formaldehyde, or methanol, on noble metal electrodes is of great interest in anodic reactions of direct electrochemical energy conversion [1–5]. Dynamical instabilities in electrochemistry most frequently arise through the interplay of the outer electrical load line and a sequence of faradaic processes with non-monotonous current–potential characteristics [6,7]. However, more important in the present context are non-stationary operation points in which the measured currents or potentials temporally exhibit autonomous electrochemical oscillations [7,8]. The origin and the existence conditions of these oscillations in electrocatalytic oxidation of fuels have recently been clarified [9–11]. The variation of the phase shift between fluxes and forces through periodic perturbations can lead to superior non-stationary operating conditions (oscillatory), enhancing the efficiency compared to stationary states [12–14]. This idea has recently attracted renewed interest in the context of electrochemical energy conversion devices [15,16]. Aside from temporal aspects, control of spatial coupling across electrified interfaces may provide interesting applications. For example, electrochemical devices are conceivable where local activation of a poisoned electrocatalytic surface is sufficient to restore complete activity, if the interface supports propagating active fronts. This result can be advantageous for operating self-poisoning processes under such dynamic conditions. It has been shown that bismuth adatoms significantly enhanced the susceptibility of the catalytic interface towards self-activation process [17].

In this work, we try to elucidate the mechanistic origin of current oscillations in the electro-oxidation of formic acid on a Pt electrode modified by bismuth deposition.

2. Experimental

A smooth polycrystalline Pt ring with inner diameter of 34.5 mm and outer diameter of 40.5 mm (thus exhibiting a geometric surface area of 7 cm^2) was used as the working electrode (WE). A concentric platinized Pt wire ring (thickness of 1 mm wire, 70 mm ring

* Corresponding author. Fax: +49-30-8413-5106.
E-mail address: jlee@fhi-berlin.mpg.de (J. Lee).

0013-4686/01/$ - see front matter
PII: S0013-4686(01)00744-7

diameter) used as counter electrode was placed 60 mm above the WE. The tip of a Luggin–Haber capillary hosting a Hg/Hg_2SO_4, K_2SO_4 (satd.) reference electrode was placed in the center of the ring working electrode. Experiments have been executed without forced convection such as magnetic stirring or nitrogen bubbling.

All solutions were prepared with ultrapure water (Millipore Milli-Q water, 18 MΩ cm) and were kept at room temperature. Before each experiment, the Pt ring WE was chemically cleaned in H_2SO_4 (Merck, suprapure):30% H_2O_2 (1:1) and a preliminary voltammetric curve between -600 and $+600$ mV (vs. Hg/Hg_2SO_4) was recorded in 0.5 M H_2SO_4 to confirm the absence of any residuals of adatoms. Cyclic voltammetry (CV) without formic acid was performed in oxygen-free H_2SO_4 solution and the sulfuric acid solution was adjusted to higher pH with addition of aqueous NaOH solution. For investigation of the electrocatalytic oxidation of formic acid, 0.1 M HCOONa (Merck, p.a.) in 0.033 M H_2SO_4 was used as the electrolyte (pH 2.85). After each experiment, the WE was treated in conc. $HClO_4$ (Merck, suprapure) to completely remove bismuth adatom residuals.

A 1×10^{-3} M Bi^{3+} containing solution was prepared by dissolution of high-purity bismuth(III) oxide (Bi_2O_3, Strem Chemicals Inc., 99.9998%) in 0.5 M $HClO_4$. Appropriate amounts of the 1×10^{-3} M Bi^{3+} solution were added to the electrolyte to adjust the desired concentrations of Bi^{3+}. Prior to each CV measurement, the initial WE potential was kept at open circuit potential of -320 mV in order to establish the same bismuth coverage of the Pt electrode.

A home-built potentiostat (Electronic Lab, Fritz-Haber-Institut der MPG) was used for all CV and chronoamperometry (CA) experiments and the data were transferred to an IBM compatible PC controlled by a GPIB interface. Galvanostatic experiments were performed by means of a bi-potentiostat (EG&G, Model 366).

For the in situ characterization of the adsorption/desorption of reducible species, rotating ring disk electrode (RRDE, Tacussel electronique) measurements were performed. Disk and ring were polycrystalline Pt. A Pt coil and a Hg/Hg_2SO_4 electrode served as counter and reference electrode, respectively. In the RRDE experiment, the Pt ring electrode was kept at -580 mV with the disk rotation set to 2000 rpm. The reported RRDE measurements plot the instantaneous deviation ΔI_{ring} of the stationary ring current I^0_{ring} versus potential.

Impedance spectra were measured at different constant outer potentials using a potentiostat and galvanostat (EG&G, PAR 273A)/log-in amplifier (NF Circuit Design Block Co., frequency response analyzer, Model S-5720). The frequency range investigated reached from 10 kHz to 0.1 Hz with 25 points per decade.

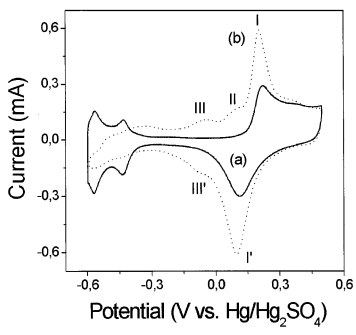

Fig. 1. Cyclic voltammetry of a Pt working electrode with a scan rate of 50 mV/s. (a) Solid line is CV without Bi^{3+} and (b) dotted line presents the CV in 0.5 M H_2SO_4 with 1×10^{-5} M Bi^{3+}.

3. Results and discussion

3.1. The study of underpotential deposition of bismuth on Pt

The effect of underpotential deposition of bismuth during cyclic voltammetry (CV) of the Pt electrode in 0.5 M H_2SO_4 is shown in Fig. 1. CV (Fig. 1b) in a solution containing 1×10^{-5} M Bi(III) shows that a high coverage of adsorbed bismuth suppresses the adsorption of hydrogen [18]. Comparing with CV on pure Pt (see Fig. 1a), several new voltammetric features on bismuth deposited Pt are obtained in the potential range between -200 mV and $+400$ mV. First of all, an asymmetric pair of oxidation peak I at $+200$ mV on the anodic scan and of reduction peak I′ at $+100$ mV on the cathodic scan is obtained. This result indicates that the formation and the reduction of Bi–oxygen species are considerably enhanced in the presence of bismuth. A plateau marked with II is also obtained on the anodic scan. Secondly, we observe a weaker reversible redox process at III and III′ discernible around -50 mV. The overall cyclic voltammetric profile on the bismuth modified Pt electrode qualitatively resembles a superposition of earlier current–potential curves obtained on Pt(100) and Pt(110) single crystals during bismuth underpotential deposition [19,20].

To investigate the adsorption/desorption behavior of the bismuth oxide species in detail, RRDE measurements of CV on bismuth modified Pt are carried out. Anodic redox peaks in the potential range of peaks I–III are commonly associated with a stepwise oxidation of adsorbed bismuth adlayers by dissociative adsorption of water [19,21,22]. The ring potential was fixed at -580 mV to ensure the reduction of the dissolved bismuth species and to avoid the evolution of hydrogen. Thus, the ring current is a measure of the

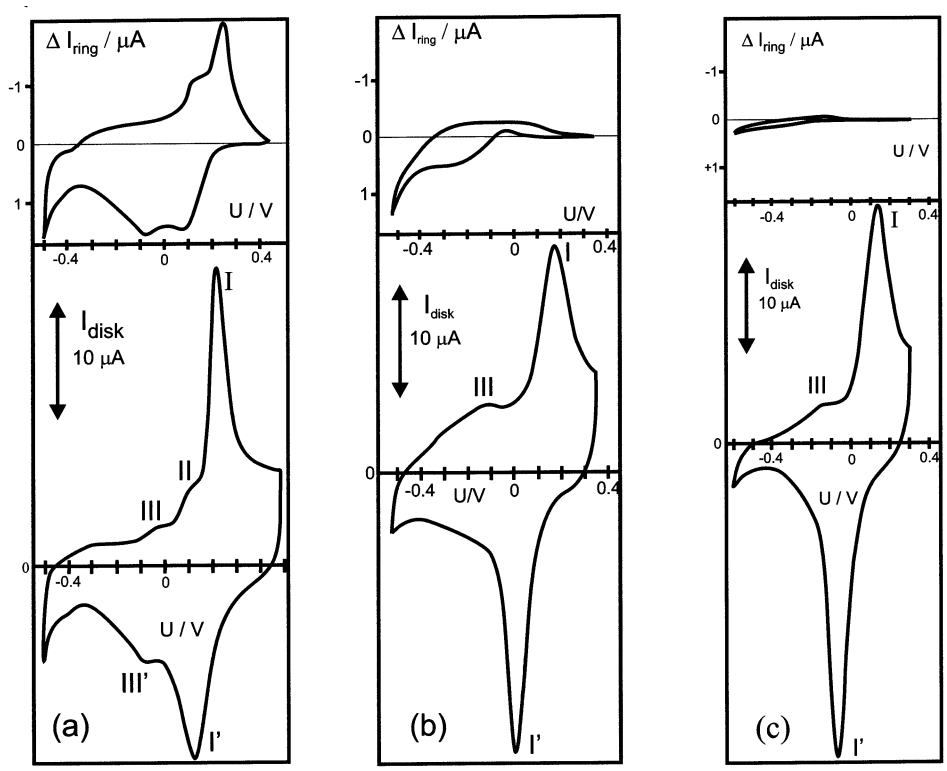

Fig. 2. RRDE analysis of Pt modified by bismuth addition with a scan rate of 50 mV/s. (a) pH 0 (0.5 M H_2SO_4); (b) pH 2; and (c) pH 3. The concentration of Bi^{3+} is 5×10^{-5} M. The ring current is proportional to the deviation of the Bi ion concentration from this value.

local Bi(III) concentration. At pH 0 (Fig. 2a), the anodic profile of the disk current (except for peak III) matches the ring profile, indicating the formation of soluble bismuth species at peaks I and II. Adsorbed metallic bismuth is most likely oxidized to species such as Bi^{3+}, $Bi(OH)_2^+$, or $Bi(OH)^{2+}$. Peak III does not have any noticeable effect on the ring signal, suggesting that adsorbed metallic bismuth is not directly involved in the redox process or the adsorbed bismuth species are insoluble. The cathodic ring signal in Fig. 2a reveals reductive bismuth adsorption between $+200$ mV (I′) and -350 mV (III′). Note that the underpotential deposition technique causes the formation of dense or even multiple bismuth adlayers by continuous adsorption of bismuth during successive voltammetric cycles. In other words, potential controlled deposition yields higher coverages than achievable under open-circuit operation. For a better understanding of the adsorption/desorption behavior of bismuth ion in HCOOH oxidation at pH 2.85, we measured the CV in 0.5 M H_2SO_4 adjusted with NaOH to higher pH.

At pH 2 and 3 (Fig. 2b and c, respectively), the voltammetric ring profile has drastically changed compared with Fig. 2a. Despite comparable disk currents, both cathodic and anodic currents at the ring decrease dramatically. Thus, at peaks II and I there is very little dissolution of bismuth at pH 3. Obviously, bismuth adlayers at peak III in Fig. 2b transformed into bismuth surface oxides with a much lower dissolution rate compared to the soluble Bi(III) species formed at pH 0 (Fig. 2a). In Fig. 2b, only a small fraction of the bismuth adlayer is dissolved near peak II, which largely coincides with peak I (-100 to 0 mV in Fig. 2b) for the Pt disk employed. Although this result confirms that Bi redox processes around peak III are not associated with the formation of any soluble and reducible Bi species, the exact nature and oxidation state of the resulting Bi species is not clear.

The above experiments on bismuth underpotential deposition reflect the following three distinct redox processes: (a) the increment of charge of peaks I and I′ compared to pure Pt electrodes involves the surface oxidation of the electrode; (b) a cathodic plateau of peak I referred to as peak II; and (c) a relatively weaker, and reversible pair of peaks III and III′ is formed. The overall voltammetric profile of the above three processes on the electrode is in good agreement with the behavior of Pt(100) or Pt(110) single crystals [19,20]. Although the Pt(111) surface is known to exhibit a single sharp redox feature around peak III/III′ [19,20,22], its contribution may be small, if not negligible, based on the relative peak heights.

Most earlier studies focusing on the bismuth-modified Pt(111) surface attributed reversible bismuth redox processes at peak III/III′ to a two-electron oxidation of metallic bismuth to a $Bi(OH)_2$ or BiO species,

depending on solution pH [19,20,22–24]. The proposed oxidation state of bismuth was solely based on charge evaluations from cyclic voltammogram. However, a recent XPS study [21] showed that bismuth adatoms did not undergo any change in oxidation state. Based on XPS data in the oxygen range, voltammetric redox features in the range of peak III/III′ were associated with the coadsorption of oxygen containing anion (OH^-). The proposed species is symbolized as (Bi_{ad}·OH^-) representing some coadsorbed state of metallic bismuth and hydroxide ions. Up to now, bismuth redox processes and pH dependencies at higher overpotentials are still not quite clear. Thus, RRDE experiments provide some information of the processes involved. At pH 0, processes II, I, and I′ are clearly associated with the dissolution and deposition of bismuth ions (Fig. 2a). These ions most likely involve species like Bi^{3+}, $Bi(OH)_2^+$ or $Bi(OH)^{2+}$ [25]. On the cathodic scan, underpotential deposition of bismuth extends to potentials of peak III′ yielding a net deposition of bismuth during CV. This has been observed previously [26] and explains the obvious asymmetry when comparing the measured cathodic and anodic ring charges in Fig. 2a–c.

3.2. Oscillatory formic acid oxidation on Pt modified by bismuth adatoms

Fig. 3 illustrates the effect of bismuth adatoms on the formic acid oxidation on Pt electrode. Fig. 3a (dotted line) shows the typical CV profile on an unmodified Pt electrode, while about five times higher electro-oxidation current of HCOOH on Bi modified Pt electrode is observed (solid line). According to previous studies [20,26–28], this higher electrocatalytic activity of Bi/Pt for HCOOH oxidation can be due to two modification effects of bismuth adatoms such as a third-body effect on Pt(100) and an electronic effect on Pt(111). In this work, polycrystalline Pt was used, and thus one can speculate that the enhanced current may be the result of both steric hindrance of the formation of poisoning species (CO) and intrinsic kinetic enhancement [29–31]. The value of the oscillatory current related with formic acid oxidation is significantly higher than that on pure Pt. This oscillation is observed over a broad potential region between +110 and +280 mV and it indicates periodic activating and passivating processes of the electrode. The potential parameter dependence of the current oscillations exhibits the following interesting features. Current oscillations with high frequency and small amplitude abruptly set in on the left flank of the peak on the anodic scan. At the onset of oscillations, a stationary I/U curve with positive slope (Fig. 3a-I) is obtained, while at higher anodic overpotential, an I/U profile with negative slope (negative differential resistance) shows higher amplitude and smaller frequency oscillation (Fig. 3a-II). Analysis of Fig. 3 suggests that the formation of bismuth surface oxides leads to a relatively rapid decline in the high currents between +220 and +280 mV. On the other hand, very high coverage of metallic bismuth (below −200 mV) decreases the oxidation current, since bismuth on the Pt electrode inhibits the adsorption of HCOOH. Interestingly, as sketched in Fig. 3 (see inset), the average value ($\langle I_{osc} \rangle$) of the oscillatory current during HCOOH oxidation on Bi/Pt electrode is higher than that of the stationary operation points at the same applied potential. Accordingly, direct formic acid or methanol oxidation under autonomous oscillatory conditions and/or by applying external pulses can lead to increased power output.

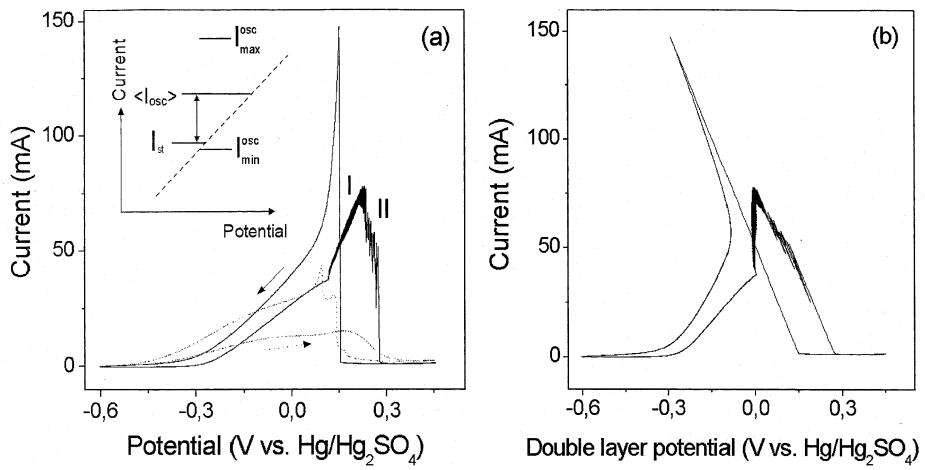

Fig. 3. (a) Cyclic voltammetry of electro-oxidation of formic acid in the absence of Bi^{3+} (dotted line) and in the presence of bismuth ion of 1×10^{-6} M (solid line). (b) *IR* correction of CV of (a) in order to allow comparison with the potentials of Bi deposition/dissolution of Figs. 1 and 2. Electrolyte is 0.1 M HCOONa/0.033 M H_2SO_4 and scan rate is 5 mV/s. The inset schematically shows that oscillatory systems can exhibit an advantage in the current yield. Extrapolation of the stationary current suggests that this may be the case in the present system.

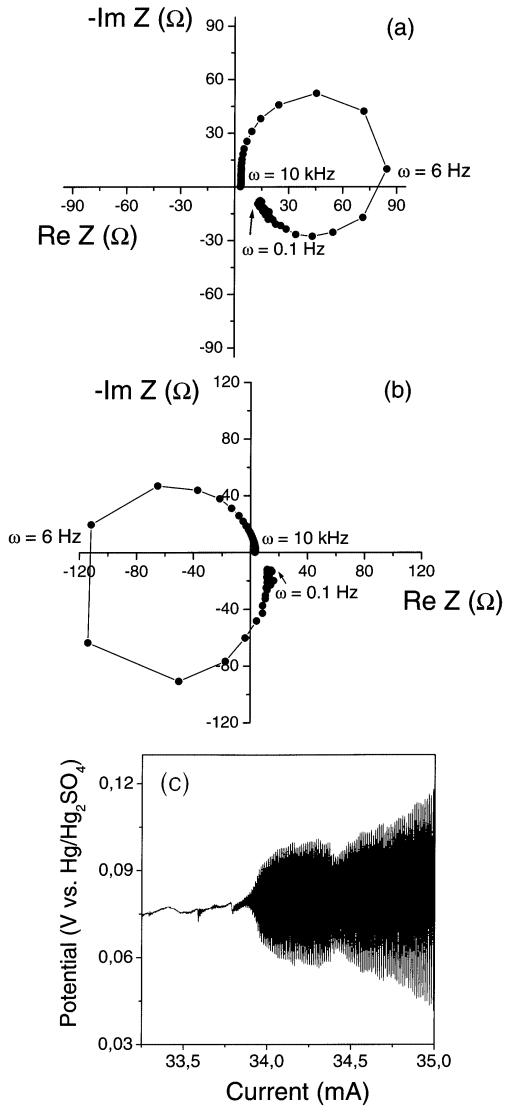

Fig. 4. Electrochemical impedance data of the HCOOH oxidation on bismuth modified Pt: (a) + 70 mV; and (b) + 80 mV. (c) Potential oscillations in the galvanostatic mode with a scan rate of 0.05 mA/s in 0.1 M HCOONa/0.033, M H_2SO_4 with 1×10^{-6}M Bi^{3+}.

To analyze the mechanistic origin of the current oscillations in Fig. 3, the electrochemical impedance spectra were measured prior to the onset of periodic oscillations. Nyquist plots at two different applied potentials U are shown in Fig. 4. At outer potential (U) of + 70 mV (Fig. 4a), the impedance plot $Z(\omega)$ exhibits a clockwise capacitive–inductive loop indicating dynamically stable stationary operating points. On the other hand, the impedance plot is drastically changed at + 80 mV in Fig. 4b. $Z(\omega)$ wraps around the origin counterclockwise, which means that we obtain the intersection between the real axis and $Z(\omega)$ where Z becomes real and negative at a finite frequency ω_0 of 5–6 Hz. $Z(\omega)$ again exhibits positive real resistances for very low frequencies. The detailed shape of the Nyquist plot bears information of the mechanistic origin of the oscillatory behavior, which can be used to predict the dynamical stability of oscillatory systems. The significance of the distinct value ω_0 in Fig. 4b where Im $Z = 0$ with Re $Z < 0$ becomes clear in galvanostatic oscillations (see Fig. 4c). A galvanostatic scan of the formic acid oxidation results in an onset potential of sustained oscillations between + 70 and + 80 mV with an initial oscillation frequency of ca. 5 Hz. As discussed in previous work [7,32,33], the critical potential, where the Nyquist plot crosses the negative real axis, marks the galvanostatic transition to periodic behavior, i.e. Hopf bifurcation. The value of ω_0 represents the intrinsic frequency of oscillation in the electrocatalytic oxidation of HCOOH on Bi/Pt.

In order to better understand the poisoning and reactivating behavior at the electrode (which need by no means occur homogeneous), we recorded the spatiotemporal evolution of the interfacial potential. Fig. 5 shows the schematic diagram of the experimental setup. The local interfacial electrode potential was recorded with microprobes placed close to the WE. The reference electrode (in the center of the ring) is close to the WE, which causes the migration coupling to become negative with increasing distance [34,35], such that opposite areas on the ring tend to be anti-correlated.

The temporal current response and a two-dimensional space–time plot of the local potential along the Pt ring electrode are shown in Fig. 6 when constant outer potential (U) is applied. A higher interfacial potential (ϕ) corresponds to low local catalytic activity due to poisoning, while low values of the interfacial

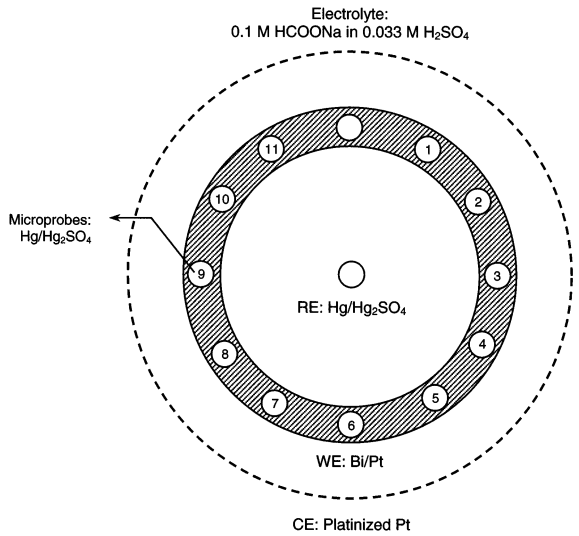

Fig. 5. Experimental setup. To monitor the instantaneous local interfacial potentials along the WE, 11 potential microprobes were equispaced along the WE. The microprobes capped with a commercial Hg/Hg_2SO_4 electrode were filled with a 0.5 M Na_2SO_4 solution (Merck, p.a.). The distance between the WE and the end of capillary of microprobes was ca. 200–300 μm. The probe signals were sampled at 1 kHz with their noise level being less than 1%.

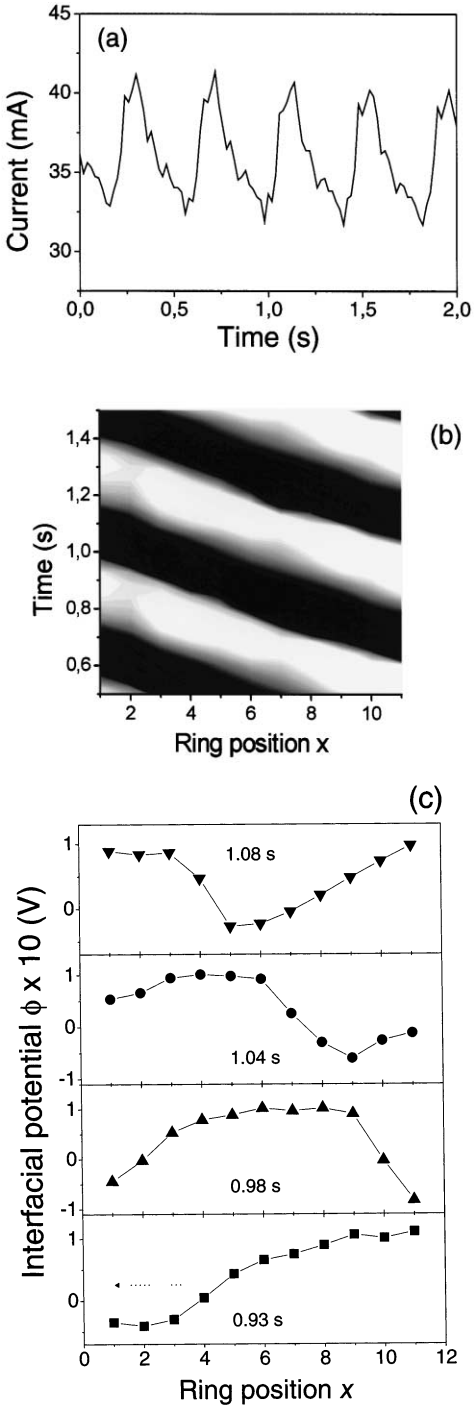

Fig. 6. (a) Current profile at constant outer potential (U) of $+150$ mV; (b) contour plot (2D) of the local interfacial potential during current oscillations; and (c) time sequence of traveling pulse along the ring Pt electrode. Black and white represent the activating and passivating state of the Pt electrode, respectively. Electrolyte is 0.1 M HCOONa/0.033 M H_2SO_4.

potential make a large contribution to the total current (active). Fig. 6a represents sustained current oscillations. Fig. 6b shows that a narrow pulse domain of high activity (black color) is continuously traveling on the ring surface. Fig. 6c exhibits a temporal sequence of the distribution of the interfacial potential on the ring electrode and it clearly shows the traveling character of an activating domain pulse. Note that the traveling pulse changes its size and shape periodically (due to imperfection of the electrode), which gives rise to oscillations in the total current.

In the formic acid oxidation on pure Pt, poisoning by adsorbed CO was shown to play an important role in the oscillation mechanism [9,10]. Adsorbed CO is removed reactively as soon as OH adsorption sets in. In the presence of Bi less CO forms and it is removed presumably by reaction with Bi–oxygen species. Thus although some CO may still be formed on Bi-modified Pt, the oscillation mechanism can be rationalized even if we neglect CO, as follows. First of all note that under the conditions in question most of the Bi is irreversibly adsorbed, which causes a significant increase in current (compared to pure Pt). In contrast, additional amounts of Bi (which reversibly deposit and redissolve) cause the current to slightly decrease again. Increasing amounts of oxygen species (most likely Bi oxides) form between 0 and 0.2 V (cf. Figs. 2c and 3b), which causes a significant current decrease. Starting at a high-current state during the oscillatory cycle near the onset, the potential ϕ is relatively low, namely between peaks III and II (cf. Figs. 2 and 3b). Here the Bi adlayer is expected to exist as a metallic state [22]. Due to potential controlled bismuth deposition, the bismuth coverage reaches values above the limit reached by irreversible open circuit potential (OCP) deposition. The resulting bismuth adlayer becomes denser [23] and causes a drop in the HCOOH current I. According to the relationship, $U = IR + \phi$, the interfacial potential ϕ now gradually rises, until at the onset of peak II, ϕ reaches a point where the reduced bismuth ad-atoms undergo a stepwise transformation to Bi(III) oxides. In a first step, the metallic Bi_{ad} is oxidized to insoluble BiO_{ad} as follows:

$$Bi_{ad}{\cdot}OH^- \rightarrow BiO_{ad} + 2e^- + H^+ \quad (1)$$

The presence of adsorbed BiO on the Pt surface decreases its catalytic activity. Therefore, ϕ increases, yielding a self-enhancing feedback loop towards higher potentials ϕ and the deactivated BiO state. In a second step, BiO_{ad} is oxidized to a Bi(III) species, which is still adsorbed on the surface,

$$BiO_{ad} \rightarrow BiO^+_{ad} + e^- \quad (2)$$

Then the adsorbed BiO^+ dissolves,

$$BiO^+_{ad} \rightarrow (BiO^+_{sol})\uparrow \quad (3)$$

Therefore, the effective coverage of bismuth oxide is reduced down to the lower limit value of irreversibly adsorbed bismuth. The oxidation current increases on the slow time scale of Bi(III) dissolution, which stops the positive feedback in ϕ. With increasing I, ϕ starts

to decrease again. At more cathodic potentials, the residual bismuth oxide is reduced and additional deposition of bismuth sets in until the bismuth adlayers reach their initial metallic state, $Bi_{ad}{\cdot}OH^-$. If one assumes that the initial oxidation step to BiO is sufficiently fast, one can expect negative impedance on this fast time scale, while positive impedance follows on a time scale of the slow Bi(III) dissolution. This is confirmed by the measured impedance curves given in Fig. 4 showing a hidden negative differential resistance (HNDR) with a non-zero frequency. As in previous work on electrochemical oscillators [7,32], the formic acid oscillator on Bi/Pt can be categorized into the mechanistic class IV of HNDR oscillators, most likely into the IV.2 subclass [32]. The above mechanistic hypothesis resembles the processes of the oscillatory H_2 oxidation on Pt in the presence of anions and electrosorbing cations [36,37], i.e. it consists of a slow process with positive and a faster with negative impedance. Further away from the onset, oscillations persist on a branch in the CV with negative differential resistance (NDR). While the irreversibly adsorbed Bi remains on the surface in this region, no additional deposition/redissolution takes place any more (cf. Fig. 2). Consequently, the mechanism is expected to be of NDR-type (class III according to Ref. [33]). The NDR is caused to increasing poisoning by adsorbed oxygen with increasing potential, the slow negative feedback loop is most likely due to the transport of HCOOH to the electrode (cf. Refs. [9,10]).

4. Conclusions

In the oxidation of formic acid on Bi/Pt, temporal periodic recovery of the activity of the electrode may lead to an increased and prolonged activity of the Pt metal electrode. Rotating ring disk electrode measurements showed that most bismuth remained on the Pt electrode at pH 3, indicating continuous enhanced electrocatalytic activity of Bi/Pt for HCOOH oxidation. A HNDR was deduced from the electrochemical impedance spectra near the onset of potential oscillations, while a manifest NDR appears to be responsible for the oscillations at higher potentials. In electrocatalytic systems with negative coupling conditions, the antiphase dynamics could prevent an entire poisoning of the electrode, since partial poisoning at some point on the electrode would enhance the catalytic activity at a remote location. With a ring electrode this effect manifests itself as traveling electrocatalytic pulses.

Acknowledgements

The authors are deeply indebted to Christian Eickes for his technical assistance with electrochemical impedance spectroscopy. Financial support by the Deutsche Forschungsgemeinschaft (DFG) through Sfb 555/B4 is gratefully acknowledged.

References

[1] M.W. Breiter, Electrochemical Processes in Fuel Cell: Anorganische und Allgemeine Chemie in Einzeldarstellungen, vol. IX, Springer, New York, 1968.
[2] W. Vielstich, Fuel Cells, Wiley, New York, 1970.
[3] R. Parsons, T. VanderNoot, J. Electroanal. Chem. 257 (1988) 9.
[4] J. Lipkowski, P.N. Ross, Electrocatalysis, Wiley-VCH, New York, 1998.
[5] S. Gottesfeld, in: R.C. Alkire, H. Gerischer, D.M. Kolb, C.W. Tobias (Eds.), Advances in Electrochemical Science and Engineering, vol. 5, Wiley-VCH, New York, 1997.
[6] M.T.M. Koper, J.H. Sluyters, J. Electroanal. Chem. 371 (1994) 149.
[7] M.T.M. Koper, Adv. Chem. Phys. 92 (1996) 161.
[8] J.L. Hudson, T.T. Tsotsis, Chem. Eng. Sci. 49 (1994) 1493.
[9] P. Strasser, M. Lübke, F. Raspel, M. Eiswirth, G. Ertl, J. Chem. Phys. 107 (1997) 979.
[10] P. Strasser, M. Eiswirth, G. Ertl, J. Chem. Phys. 107 (1997) 991.
[11] M. Schell, X. Cai, Electrochim. Acta 38 (1993) 519.
[12] J. Lazar, J. Ross, J. Chem. Phys. 92 (1990) 3579.
[13] A. Hjelmfelt, L. Schreiber, J. Ross, J. Phys. Chem. 95 (1991) 6048.
[14] J.F. Hervagault, J.G. Lazar, J. Ross, Proc. Natl. Acad. Sci. USA 86 (1989) 9258.
[15] D. Wilkinson et al., US Patent 6,096,448 (2000).
[16] M. Schell, F.N. Albahadily, J. Safer, J. Electroanal. Chem. 353 (1993) 303.
[17] S. Smith, K. Ben-Dor, H. Abruna, Langmuir 15 (1999) 7325.
[18] A. Holleman, E. Wiberg, Lehrbuch der Anorganischen Chemie, Walter de Gruyter, Berlin, 1985.
[19] J. Clavillier, J. Feliu, A. Aldaz, J. Electroanal. Chem. 243 (1988) 419.
[20] S. Chang, Y. Ho, M. Weaver, Surf. Sci. 265 (1992) 81.
[21] U. Hamm, D. Kramer, R. Zhai, D.M. Kolb, Electrochim. Acta 43 (1998) 2969.
[22] S. Chang, M. Weaver, Surf. Sci. 241 (1991) 11.
[23] J. Feliu, A. Fernandez-Vega, J. Orts, A. Aldaz, J. Chem. Phys. 88 (1991) 1493.
[24] J. Clavilier, A. Fernandez-Vega, A. Aldaz, J. Electroanal. Chem. 258 (1989) 89.
[25] B. Lovrecek, M. Metikos-Hukovic, I. Mekajavic, in: A.J. Bard (Ed.), Encyclopedia of Electrochemistry of the Elements, vol. 9, Marcel Dekker, New York, 1986.
[26] E. Herrero, J.M. Feliu, A. Aldaz, J. Electroanal. Chem. 368 (1994) 101.
[27] T.D. Jarvi, E.M. Stuve, in: J. Lipkowski, P.N. Ross (Eds.), Electrocatalysis, Wiley-VCH, New York, 1998, p. 75.
[28] E. Herrero, A. Fernandez-Vega, J.M. Feliu, A. Aldaz, J. Electroanal. Chem. 350 (1993) 73.
[29] M. Watanabe, S. Motoo, J. Electroanal. Chem. 60 (1975) 267.
[30] M. Shibata, O. Takahashi, S. Motoo, J. Electroanal. Chem. 249 (1988) 253.
[31] M. Shibata, N. Furuya, M. Watanabe, S. Motoo, J. Electroanal. Chem. 263 (1989) 97.
[32] P. Strasser, M. Eiswirth, M.T.M. Koper, J. Electroanal. Chem. 478 (1999) 50.
[33] M.T.M. Koper, J. Electroanal. Chem. 409 (1996) 175.

[34] J. Christoph, R.D. Otterstedt, M. Eiswirth, N.I. Jaeger, J.L. Hudson, J. Chem. Phys. 110 (1999) 8614.
[35] J. Christoph, P. Strasser, M. Eiswirth, G. Ertl, Science 284 (1999) 291.
[36] W. Wolf, K. Krischer, M. Lübke, M. Eiswirth, G. Ertl, J. Electroanal. Chem. 385 (1995) 85.
[37] W. Wolf, M. Lübke, M.T.M. Koper, K. Krischer, M. Eiswirth, G. Ertl, J. Electroanal. Chem. 399 (1995) 185.